



HAL
open science

ERR α coordinates actin and focal adhesion dynamics

Violaine Tribollet, Catherine Cerutti, Alain G elo en, Emmanuelle Berger,
Richard de Mets, Martial Balland, Julien Courchet, Jean-Marc Vanacker,
Christelle Forcet

► **To cite this version:**

Violaine Tribollet, Catherine Cerutti, Alain G elo en, Emmanuelle Berger, Richard de Mets, et al..
ERR α coordinates actin and focal adhesion dynamics. *Cancer Gene Therapy*, 2022, 29 (10), pp.1429-
1438. 10.1038/s41417-022-00461-6 . hal-04176612

HAL Id: hal-04176612

<https://hal.science/hal-04176612v1>

Submitted on 3 Aug 2023

HAL is a multi-disciplinary open access archive for the deposit and dissemination of scientific research documents, whether they are published or not. The documents may come from teaching and research institutions in France or abroad, or from public or private research centers.

L'archive ouverte pluridisciplinaire **HAL**, est destin ee au d ep ot et  a la diffusion de documents scientifiques de niveau recherche, publi es ou non,  emanant des  tablissements d'enseignement et de recherche fran ais ou  trangers, des laboratoires publics ou priv es.

ERR α coordinates actin and focal adhesion dynamics

Violaine Tribollet¹, Catherine Cerutti¹, Alain G elo en², Emmanuelle Berger²,
Richard De Mets³, Martial Balland⁴, Julien Courchet⁵, Jean-Marc Vanacker¹ and
Christelle Forcet¹.

¹Institut de G enomique Fonctionnelle de Lyon, Universit  de Lyon, Universit  Claude
Bernard Lyon 1, CNRS UMR5242, Ecole Normale Sup rieure de Lyon, 69007 Lyon,
France.

²UMR Ecologie Microbienne, Universit  de Lyon, CNRS 5557, INRA 1418, VetAgro Sup,
Universit  Claude Bernard Lyon 1, 69622 Villeurbanne cedex, France.

³Mechanobiology Institute, National University of Singapore, Singapore 117411.

⁴Laboratoire Interdisciplinaire de Physique, Grenoble Alpes University, 38402 Saint
Martin d'H eres, France.

⁵Institut NeuroMyoG ne, Universit  de Lyon, Universit  Claude Bernard Lyon 1, CNRS
UMR-5310, INSERM U-1217, 69008 Lyon, France.

Correspondence should be addressed to C. F. (christelle.forcet@ens-lyon.fr, Tel: +33
(0)4 26 73 13 46, Fax: +33 (0)4 26 73 13 75).

Abstract

Cell migration depends on the dynamic organization of the actin cytoskeleton and
assembly and disassembly of focal adhesions (FA). However the precise mechanisms
coordinating these processes remain poorly understood. We previously identified the
estrogen-related receptor α (ERR α) as a major regulator of cell migration. Here, we
show that loss of ERR α leads to abnormal accumulation of actin filaments that is
associated with an increased level of inactive form of the actin-depolymerising factor

26 cofilin. We further show that $ERR\alpha$ depletion decreases cell adhesion and results in
27 defective FA formation and turnover. Interestingly, specific inhibition of the RhoA-
28 ROCK-LIMK-cofilin pathway rescues the actin polymerisation defects resulting from
29 $ERR\alpha$ silencing, but not cell adhesion. Instead we found that MAP4K4 is a direct target of
30 $ERR\alpha$ and down-regulation of its activity rescues cell adhesion and FA formation in the
31 $ERR\alpha$ -depleted cells. Altogether, our results highlight a crucial role of $ERR\alpha$ in
32 coordinating the dynamic of actin network and focal adhesion through the independent
33 regulation of the RhoA and MAP4K4 pathways.

34

35 Key words: actin, focal adhesion, RhoA, MAP4K4, $ERR\alpha$

36

37 **Introduction**

38 Cell migration is essential for embryonic development, wound healing and immune
39 response (1). Its dysregulation contributes to many pathologies including cancer cell
40 dissemination (2).

41 The multistep process of cell movement requires highly coordinated changes in cell
42 morphology and interactions with the extracellular matrix (ECM). Cell migration can be
43 divided into four discrete steps: formation of protrusion, adhesion to the ECM,
44 generation of traction forces at the adhesion sites and release of adhesion at the rear,
45 which allow the cell to move forward (1,3). The growing actin network pushes the
46 membrane and promotes lamellipodial protrusion at the leading edge. Protrusions are
47 then stabilised by integrin-based protein complexes known as focal adhesions (FA)
48 connecting the actin cytoskeleton to the ECM. In addition, actomyosin fibers contribute
49 to the contraction and the retraction of the cell body. Therefore this sequence of events

50 involves a dynamic organization of the actin cytoskeleton and a controlled assembly and
51 disassembly of FA that must be coordinated both in space and time (1,4,5).

52 The Rho GTPases plays a major role in regulating the actin cytoskeleton and cell
53 migration (6–8). Notably, RhoA initiates the process by inducing actin assembly at the
54 cell front and mediates the interaction of contractile actin-myosin filaments that
55 promotes FA maturation, cell body translocation and rear retraction (8–11). RhoA
56 promotes actin assembly through its effectors mammalian homolog of *Drosophila*
57 diaphanous (mDIA) and Rho-associated protein kinase (ROCK) (6,12). mDIA initiates
58 actin filament assembly by nucleation, whereas ROCK promotes actin polymerisation
59 through the activation of the LIM kinase (LIMK) resulting in the inhibition of the actin-
60 severing activity of cofilin (13,14).

61 The mitogen-activated protein kinase kinase kinase kinase (MAP4K4) has also been
62 shown to be involved in cell migration, in particular by specifically controlling FA
63 dynamics (15,16). Interestingly, microtubules serve as tracks to deliver proteins that act
64 locally at FA to promote their turnover (11,17). In this way, MAP4K4 is delivered to FA
65 sites to induce the activation of the GTPase Arf6 which promotes integrin internalization
66 from the cell surface and FA turnover (18). MAP4K4 also regulates FA disassembly in
67 migrating cells by phosphorylating moesin, which displaces talin from integrins and
68 induces their inactivation (19). Furthermore, the pro-migratory function of MAP4K4
69 relies on its ability to induce endocytosis and activation of the integrin β 1 adhesion
70 receptor (20). Overall, cell migration is a complex and dynamic phenomenon, which
71 involves crosstalks between actin and FA. However, how these processes are
72 coordinated to support cell migration is not clearly understood.

73 Our team and others have demonstrated that the estrogen-related receptor α (ERR α)
74 is an important factor promoting cell migration (21–23). ERR α is an orphan member of

75 the nuclear receptor superfamily and acts as a transcription factor (24,25). ERR α is
76 strongly expressed in several types of cancers and its high expression correlates with
77 poor prognosis (23,25,26). In addition, accumulating evidence indicates that ERR α plays
78 a major role in tumoral growth and progression via stimulation of cell proliferation
79 (27,28), angiogenesis (29–32), aerobic glycolysis (33,34) and ECM invasion (35,36). In
80 breast cancer cells, we previously showed that ERR α promotes directional cell
81 migration by regulating RhoA stability and activity (22). Consequently, the invalidation
82 of ERR α leads to impaired cell migration which is associated with cell disorientation,
83 disorganized actin filaments and defective lamellipodium formation (22). Yet the
84 specific roles of ERR α in the regulation of the discrete processes involved in cancer cell
85 migration, such as actin- and FA dynamics, remain unclear.

86 In the present study, we report that ERR α controls actin polymerisation and
87 organisation by modulating cofilin activity through the RhoA-ROCK-LIMK pathway. We
88 also found that ERR α promotes cell adhesion independently of its role on the actin
89 cytoskeleton. Indeed, ERR α directly regulates the expression of MAP4K4, and thereby
90 contributes to the modulation of FA formation and turnover. Together, our study
91 identifies ERR α as a major actor involved in the coordination of actin and FA dynamics
92 that may contribute to efficient cancer cell migration and metastasis.

93

94 **Results**

95 **ERR α regulates actin dynamics**

96 To investigate the potential role of ERR α in the regulation of actin polymerisation, we
97 first performed differential sedimentation of actin filaments (F-actin) and actin
98 monomers (G-actin) using ultracentrifugation. We observed that inactivation of ERR α

99 with a specific siRNA induced a significant increase in F-actin level with stable G-actin
100 level in both MDA-MB231 cells (Figure 1A) and HeLa cells (Figure S1A).
101 Immunofluorescence experiments showed that actin filaments are highly concentrated
102 at the cell periphery in both the control and ERR α -depleted conditions. Interestingly,
103 these actin filaments seemed to be particularly disorganized in the ERR α -depleted cells
104 (Figure 1B). In addition, quantitative image analysis revealed that the F-actin content
105 significantly increased upon ERR α depletion (Figure 1C).

106 In order to further analyse defects in actin filaments associated with ERR α
107 depletion, we used triangle-shaped micropatterns. When control cells adhered on these
108 micropatterns, they spread and acquired a triangular shape. Actin filaments
109 accumulated in these cells at the lateral edges of the triangle. By contrast, ERR α -
110 depleted cells displayed a random localization of the actin filaments and a strongly
111 altered triangular morphology (Figure 1D). Once again, depletion of ERR α induced an
112 increase in the F-actin content as compared to the control condition (Figure 1E). Taken
113 together, these results demonstrate that ERR α regulates polymerisation of actin
114 filaments.

115

116 **ERR α acts on the RhoA-ROCK pathway to modulate actin polymerisation**

117 The small GTPase protein RhoA plays a major role in regulating the organization of the
118 actin cytoskeleton through its effectors mDIA and ROCK (12,14). Downstream of ROCK,
119 the activation of LIMK results in cofilin inactivation and consecutive increase in actin
120 polymerisation (13,14). We previously showed that ERR α regulates cell migration by
121 modulating RhoA protein expression and activation of the RhoA-ROCK pathway (22).
122 We therefore investigated if the effects of ERR α on the actin cytoskeleton could result
123 from LIMK-dependent cofilin inhibition. Western blot experiments showed that

124 depletion of ERR α strongly increased the level of the inactive phosphorylated form of
125 cofilin, whereas total levels of cofilin remained unchanged (Figure 2A). The level of
126 RhoA also strongly increased in ERR α -depleted cells, as expected (Figure 2B and Figure
127 S1B). In addition, treatment with the selective ROCK inhibitor Y27632 decreased the
128 phosphorylation level of cofilin in both control and ERR α -depleted cells (Figure 2C).
129 Interestingly, this treatment was able to put the phosphorylation level of cofilin in
130 ERR α -depleted cells close to the one observed in control cells. Furthermore, the specific
131 LIMK inhibitor Pyr1 similarly rescued the phosphorylation level of cofilin in these cells
132 (Figure 2D). These findings indicate that the RhoA-ROCK-LIMK pathway is involved in
133 ERR α -mediated controls of cofilin activity. We next investigated whether the
134 deregulation of this pathway may account for the defective actin regulation observed in
135 ERR α -depleted cells. Treating micropatterned cells with 5 μ M Y27632 rescued, at least
136 partially, the increase in F-actin intensity induced by ERR depletion (Figure 2E),
137 indicating that the effect of the receptor on the RhoA-ROCK cascade is instrumental in
138 regulating the F-actin content.

139

140 **ERR α regulates cell adhesion**

141 Actin filament- and FA dynamics are tightly linked. Notably, Rho GTPases and actin
142 dynamics play a crucial role in regulating FA maturation and turnover (37–39).
143 Therefore, we determined whether ERR α is able to regulate cell adhesion through its
144 action on the RhoA pathway. Using the xCELLigence system, which allows real-time
145 monitoring of cell adhesion (40), we first showed that depletion of endogenous ERR α
146 resulted in a significant decrease in cell adhesion to collagen I compared to control
147 condition (Figure 3A). Similar effects were observed after depletion of ERR α in HeLa
148 cells (Figure S1C). We also observed that cell adhesion to collagen IV or fibronectin

149 decreased upon $ERR\alpha$ silencing (Figure 3B). By contrast, control and $ERR\alpha$ -depleted
150 cells were not able to adhere on the positively charged poly-L-lysine substrate, showing
151 that the adhesion of MDA-MB231 cells does not rely on electrostatic interactions (Figure
152 S1D). To investigate whether the upregulation of the RhoA pathway due to $ERR\alpha$
153 depletion could lead to defective cell adhesion, we then tested the effect of the ROCK
154 inhibitor Y27632 on the adhesion of $ERR\alpha$ -depleted cells. Y27632 treatment
155 exacerbated, rather than rescued, the adhesion defect of $ERR\alpha$ -depleted cells. It also
156 induced a decrease, albeit moderate, of cell adhesion under control conditions (Figure
157 3C). Treatment with the LIMK inhibitor Pyr1 also markedly reduced adhesion of the
158 control and $ERR\alpha$ -depleted cells (Figure S1E). Notably, RhoA stimulates actomyosin
159 contractility through ROCK that is required for cell adhesion (8). We thus tested the
160 possibility that abnormal actomyosin contractility resulting from $ERR\alpha$ depletion may
161 impact this process. We found that the specific myosin II inhibitor blebbistatin did not
162 change the adhesion ability of $ERR\alpha$ -depleted cells but slightly reduced adhesion of the
163 control cells (Figure S1F). Taken together, these observations suggest that a correct
164 level of activation of RhoA pathway and a precise control of the actomyosin contractility
165 contribute to optimal cell adhesion in control conditions. Our result further indicate that
166 the RhoA-ROCK pathway is not involved in $ERR\alpha$ -mediated regulation of cell adhesion.

167 FA represent the major sites of cell attachment to the ECM (1,5). Therefore, to
168 determine how $ERR\alpha$ impacts on cell adhesion, we analysed FA using vinculin as a
169 marker. Immunofluorescence microscopy showed that FA appeared smaller in $ERR\alpha$ -
170 depleted cells as compared to control cells (Figure 4A). Quantitative analysis of vinculin
171 staining revealed indeed a significant decrease of FA area and length upon $ERR\alpha$
172 depletion (Figure 4B and 4C). The distance of FA to the cell periphery was also impaired

173 in these cells, reflecting FA mislocalization (Figure 4D). To determine the potential role
174 of ERR α in FA dynamics, we next used MDA-MB231 cells stably expressing GFP-paxillin,
175 a fluorescent FA marker protein. As for their wild type counterparts, adhesion of these
176 cells to collagen I decreased upon ERR α depletion, demonstrating that the GFP tag did
177 not compromise ERR α involvement in cell adhesion (Figure S3A). We performed live-
178 cell imaging and we observed that FA displayed more rapid phases of assembly and
179 disassembly in ERR α -depleted cells as compared to control cells. Representative
180 examples of these perturbations in FA dynamics are shown in montages in Figure 4E
181 (red arrows). Quantification of the kinetics of individual FA demonstrated that depletion
182 of ERR α resulted in a significant increase in both the assembly and disassembly rates of
183 FA (Figure 4F). Altogether, these data indicate that ERR α promotes cell adhesion by
184 modulation of FA formation and turnover.

185

186 **ERR α regulates FA dynamics via its transcriptional target MAP4K4**

187 To investigate the molecular mechanisms through which ERR α controls cell adhesion,
188 we examined its transcriptional targets. Transcriptomic and Gene Ontology (GO)
189 analyses have been previously performed to identify ERR α target genes and associated
190 biological functions (22). Of particular interest, these analyses revealed MAP4K4, which
191 encodes a Ser/Thr kinase involved in the regulation of FA dynamics and cell migration
192 (15,18,19). RT-qPCR experiments verified our finding, showing that silencing of ERR α
193 led to an up-regulation of MAP4K4 expression at the mRNA level (Figure 5A).
194 Examination of publicly available chromatin immunoprecipitation sequencing (ChIP-
195 Seq) data performed on BT-474 cells (41) indicated the recruitment of ERR α on two
196 distinct regions of intron 2 of the MAP4K4 gene, each displaying two putative ERR α
197 response elements (ERREs) (Figure S2A). ChIP-qPCR experiments revealed that ERR α

198 binds these regions in MDA-MB231 cells (Figure 5B). Next, an up-regulation of the
199 MAP4K4 protein expression resulting from $ERR\alpha$ -depletion was confirmed by Western
200 blot (Figure 5C). Similar results were observed in HeLa and MDA-MB231 GFP-paxillin
201 cells (Figure S2B). Consistently, an enhanced activity of MAP4K4 was observed in $ERR\alpha$
202 depleted cells, as indicated by an increased phosphorylation of moesin, a substrate of
203 MAP4K4 involved in FA turnover (Figure 5D) (19). Together, these data demonstrate
204 that $ERR\alpha$ directly reduces the expression of MAP4K4 and consequently influences its
205 activity. Interestingly, we showed that loss of $ERR\alpha$ reduced the adhesion of BT474 cells
206 on the collagen I substrate (Figure S3B), and increased the expression of the MAP4K4
207 protein in these cells (Figure S2B), suggesting that similar molecular mechanisms are
208 involved in the adhesion of MDA-MB231, HeLa and BT474 cells.

209 MAP4K4 promotes FA disassembly by inducing integrin recycling (18) and
210 inactivation (19). These data raise the possibility that the over-activation of MAP4K4
211 observed in $ERR\alpha$ -depleted cells may account for the defects of FA identified in these
212 cells. To investigate this hypothesis, we suppressed endogenous expression of MAP4K4
213 in MDA-MB231 cells using siRNA targeting and we tested the ability of these cells to
214 adhere to collagen I substrate. Unexpectedly, our results showed that the MAP4K4
215 knockdown induced a decrease in cell adhesion as compared to control conditions
216 (Figure S3C). These data are contradictory with those of other teams which
217 demonstrated an increased cell adhesion resulting from siRNA-mediated depletion of
218 MAP4K4 in human umbilical vein endothelial cells or knockout of MAP4K4 in mice
219 keratinocytes (18,42). However, it has been suggested that MAP4K4 could play a
220 positive role in cell adhesion through protein interactions mediated by its C-terminal
221 domain (15,43). This explains why deletion of MAP4K4 may impinge on the correct
222 adhesion of cells as observed in our conditions. Therefore, since the depletion of

223 MAP4K4 may lead to cell-type-specific effects, we choose to use specific MAP4K4
224 inhibitors to analyse the potential role of MAP4K4 in $ERR\alpha$ -mediated regulation of cell
225 adhesion. First, cells were treated with the MAP4K4 inhibitor PF-06260933 (44). We
226 found that a low concentration of PF-06260933 rescued cell adhesion on the collagen I
227 substrate (Figure 6A) and restored FA area and length in $ERR\alpha$ -depleted cells (Figure 6B
228 and 6C). PF-06260933 also nearly completely rescued the relative distance of FA to the
229 cell periphery which was impaired in these cells probably due to mislocalized MAP4K4
230 activity (19), but altered FA localization in control cells (Figure 6D). Second, we
231 observed that treatment with another MAP4K4 inhibitor, GNE-495 (42,45), also rescued
232 adhesion of the $ERR\alpha$ -depleted cells (Figure S3D). Together, these data demonstrate that
233 $ERR\alpha$ regulates cell adhesion through MAP4K4.

234 As shown above, impacting on the RhoA-ROCK axis in $ERR\alpha$ -depleted cells
235 rescued the defects in actin polymerisation but not the reduced adhesion capacities. We
236 thus examined the converse possibility, questioning whether impacting on the MAP4K4
237 axis could reduce the increased actin polymerisation observed upon $ERR\alpha$ inactivation.
238 As shown on Figure 6E, treatment with the MAP4K4 inhibitor PF-06260933 did not
239 rescue the actin status in $ERR\alpha$ -depleted cells but rather increased actin polymerisation
240 in control cells. Altogether our data show that $ERR\alpha$ regulates actin polymerisation and
241 FA dynamics via two independent pathways.

242

243 **Discussion**

244 $ERR\alpha$ regulates many cellular processes contributing to tumor development and
245 progression. Most of all, $ERR\alpha$ has been largely implicated in inducing migratory and
246 invasive properties of cancer cells (21-23,35-36). $ERR\alpha$ also contributes to cell

247 migration under physiological conditions such as morphogenetic movements during
248 gastrulation of the zebrafish embryo and chemotactic migration of activated
249 macrophages (22,46). Although some molecular mechanisms through which $ERR\alpha$
250 promotes cell movements have been described, how these signalling actors are
251 connected to the precise morphological changes required for cell migration per se is still
252 unclear. In this report, we show that $ERR\alpha$ coordinates actin and FA dynamics, through
253 the independent modulation of the RhoA-ROCK-LIMK-cofilin pathway and MAP4K4
254 activity respectively.

255 A proper interaction between cells and ECM is an essential prerequisite for cell
256 migration, and it needs to be precisely regulated. Nascent adhesion complexes recruit
257 actin-binding proteins to establish a link between ECM and the actin cytoskeleton (1).
258 RhoA contributes to FA maturation by controlling the growth of FA-associated actin
259 filaments through the activation of the formin mDia and inhibition of severing activity of
260 cofilin (7,13,14). RhoA also regulates actin binding to myosin II filaments via ROCK,
261 which subsequently induces contractility required for FA maturation (8,11). We
262 previously reported that $ERR\alpha$ depletion significantly increases RhoA expression and
263 activation (22). We show here that the upregulation of RhoA activity induces an increase
264 in actin polymerisation resulting from an enhanced phosphorylation status of the ROCK
265 downstream target cofilin. This suggests that an excess of actin filaments may impair
266 their interaction with FA and impact on FA maturation. Unexpectedly, our results reveal
267 that the RhoA-ROCK pathway does not contribute to the regulation of cell adhesion
268 downstream of $ERR\alpha$. Therefore, global deregulation of RhoA activity due to $ERR\alpha$
269 depletion does not seem to have a strong influence on the precise control of actin
270 polymerisation at the FA sites.

271 It has been reported that cofilin and myosin compete for binding to actin
272 filaments (14). We demonstrate here that upregulation of the RhoA-ROCK pathway
273 leads to an increase in cofilin phosphorylation in the ERR α -depleted cells, which has
274 been shown to inhibit its interaction with actin. As a consequence, depletion or
275 inhibition of cofilin may promote actomyosin assembly (14). In addition, we previously
276 showed that the overactivation of ROCK resulting from ERR α depletion leads to an
277 increased phosphorylation of MYPT1, one of the subunits of the myosin light chain
278 phosphatase (22). In addition, an overactivation of ROCK can increase the myosin II
279 ATPase activity through phosphorylation of myosin light chain (MLC) (47). Altogether
280 these data suggest that ERR α functions as a regulator of actomyosin contractility by
281 controlling the RhoA-ROCK pathway. Therefore, ERR α may modulate the formation of
282 actin stress fibers not only through LIMK and cofilin, but also through myosin II.
283 However, in accordance with the results obtained for the RhoA pathway, we
284 demonstrate that ERR α does not promote cell adhesion through its potential effect on
285 actomyosin filaments.

286 Upon ERR α silencing, cell adhesion decreases as a result from impaired FA
287 formation and dynamics. These defects can be rescued by down-modulating the activity
288 of MAP4K4. Interestingly, we show that ERR α depletion increases both FA assembly and
289 FA disassembly. This is consistent with a report showing that loss of MAP4K4 exerts the
290 inverse effect on FA dynamics (18). MAP4K4 has been previously identified as a FA
291 disassembly factor (18,19). Nevertheless it has been recently reported that MAP4K4
292 promotes the activation of β 1-integrin and its downstream effector Focal Adhesion
293 Kinase (FAK) (48), suggesting that it may also regulate FA assembly. Therefore, further
294 investigations will be needed to determine the potential contribution of these MAP4K4-
295 dependent mechanisms in the regulation of FA assembly and maturation by ERR α .

296 MAP4K4 regulates FA dynamics by promoting internalization and inactivation of
297 β 1-integrin (18,19). In migrating cells, MAP4K4 is delivered to FA sites through its
298 association with the microtubule end-binding protein EB2 (ending binding 2). MAP4K4
299 subsequently activates IQSEC1 (IQ motif and SEC7 domain-containing protein 1) and
300 Arf6 to induce FA disassembly and cell migration (18). Furthermore, MAP4K4 is
301 involved in phosphorylation of moesin, which competes with talin for binding to β 1-
302 integrin. This leads to β 1-integrin inactivation and FA disassembly (19). Since we
303 observed the activation of moesin in the $ERR\alpha$ -depleted cells, our results strongly
304 suggest that $ERR\alpha$ reduces FA disassembly through the MAP4K4-moesin pathway. We
305 cannot completely exclude the possibility that $ERR\alpha$ also regulates FA disassembly via
306 the regulation of IQSEC1 and Arf6 activation. However, $ERR\alpha$ is more probably involved
307 in the regulation of integrin inactivation rather than their recycling because surface
308 expression of β 1-integrin (and other tested integrins) is not modified upon $ERR\alpha$
309 depletion (Tribollet and Forcet, unpublished). Furthermore, $ERR\alpha$ promotes cell
310 adhesion to different ECM proteins, suggesting the involvement of the MAP4K4-moesin
311 pathway in the regulation of distinct types of integrins. In line with that observation, the
312 role of talin in activation of multiple integrins been reported (49,50). Therefore, it is
313 plausible that $ERR\alpha$, by inducing moesin competition with talin via MAP4K4, has a more
314 general role in the regulation of integrin activation and FA turnover.

315 We previously performed a transcriptomic analysis of breast cancer cells that led
316 us to identify MAP4K4 as an $ERR\alpha$ -target gene (22). This analysis showed that the
317 expression of MAP4K4 increased by about 80% upon $ERR\alpha$ depletion, and also revealed
318 that its expression was decreased but not fully suppressed in the control condition.
319 Thus, we postulate that a correct protein level of MAP4K4 is critical for cell migration. It

320 has been shown that the knockout or the knockdown of MAP4K4 leads to FA
321 stabilisation and impaired or reduced cell migration probably due to a strong
322 attachment of the cells to the substrate (18,42). On the contrary, a marked increase in
323 expression of MAP4K4 resulting from ERR α depletion leads to FA disassembly and may
324 result in a reduced capacity of cells to respond to extracellular matrix cues.
325 Consequently, the directionality of cell migration may be impaired rather than the
326 migration process per se (22,51). We therefore propose that ERR α is important in
327 ensuring a correct level of MAP4K4 necessary for proper oriented cell migration.

328 A role of MAP4K4 in regulation of cortical actin dynamics has been previously
329 shown (52–54). Notably, these data show that MAP4K4 silencing decreases the
330 accumulation of actin filaments in cell protrusions. Thus, it suggests that the
331 upregulation of MAP4K4 resulting from ERR α depletion may promote aberrant actin
332 polymerisation. However, we demonstrate here that MAP4K4 is not involved in the
333 regulation of the actin network downstream of ERR α . Therefore, we speculate that
334 ERR α -mediated regulation of MAP4K4 expression plays a major role in cell adhesion,
335 but that another upstream signal may be needed to activate MAP4K4-dependent actin
336 polymerisation. In this way, it has been shown that MAP4K4, or its mouse homolog NIK,
337 phosphorylates ARP2 and the ERM proteins to induce actin polymerisation in response
338 to growth factor stimulation (43,52,53). Altogether, our data firmly demonstrate that
339 ERR α coordinates actin polymerisation and adhesion via two independent pathways.

340 Both ERR α and MAP4K4 have been shown to be highly expressed in cancers
341 (15,23). Our data demonstrate here that ERR α is a key transcriptional regulator of the
342 MAP4K4 gene. However, epigenetic modifications and other signalling pathways also
343 appear to be involved in the modulation of MAP4K4 expression (15). In these
344 conditions, compensation mechanisms may bypass the MAP4K4-induced cell adhesion

345 defects to facilitate oriented migration of cancer cells. Thus, this study revealed that the
346 modulation of cell adhesion exerted by $ERR\alpha$ through MAP4K4 is one specific way to
347 control breast cancer cell migration.

348 In conclusion, we report that $ERR\alpha$ modulates actin polymerization through the
349 RhoA-ROCK axis and FA formation and turnover through the MAP4K4 pathway. As a
350 consequence, deregulation of $ERR\alpha$ expression deeply impacts cell adhesion and cell
351 morphology, pointing to a critical role played by $ERR\alpha$ in cancer cell migration.

352

353 **Acknowledgements and funding sources**

354 The authors warmly thank members of the Vanacker lab for support and discussion, as
355 well as Séverine Périan for technical assistance. We are grateful to Sandrine Etienne-
356 Manneville (Institut Curie) and Laurence Lafanechère (Institute for Advanced
357 Biosciences) for reagents. We also thank the staff of PLATIM (UMS3444/CNRS,
358 US8/INSERM, ENS de Lyon, UCBL) and IGFL microscopy facilities for their precious help
359 with microscopy studies. Work in our laboratory is funded by Ligue contre le Cancer
360 (comité Rhône), Région Auvergne Rhône Alpes (grant SCUSI OPE2017_004), ANSES
361 (grant EST15-076), and ENS Lyon (programme JoRISS).

362

363 **Author contributions**

364 V.T., J.-M.V. and C.F. designed research; V.T., C.C., E.D.-B, J.C. and C.F. performed research;
365 R.D.M., M. B., and A.G. contributed to analytic tools; V.T., C.C., J.-M.V. and C.F. analyzed
366 data; and C.F. wrote the paper.

367

368 **Declaration of Interests**

369 The authors declare no competing interests.

370

371 **Materials and methods**

372 **Data and Code Availability**

373 FA quantification was done using a Matlab (MathWorks, Natick, MA) algorithm
374 developed by M. Balland and R. Demets, and the corresponding source code can be
375 found in GitHub: https://github.com/rdemets/FA_Quantif_Matlab.

376 The source code of the Focal Adhesion Analysis Server developed by M Berginski is also
377 available in GitHub: <https://github.com/mbergins/>.

378

379 **Cell lines**

380 Mycoplasma-free MDA-MB231, HeLa and BT474 cells were cultured in 4.5 g/l glucose
381 DMEM supplemented with 10% FCS (Gibco), 10 U/ml penicillin (Gibco) and 10 µg/ml
382 streptomycin (Gibco). Cells were maintained in a 5% CO₂ atmosphere at 37°C. MDA-
383 MB231 cells were transfected with pEGFP-paxillin plasmid (a generous gift from
384 Sandrine Etienne-Manneville, Institut Curie, Paris, France), selected with 1 mg/ml G418
385 (Sigma-Aldrich) and maintained as cell populations.

386

387 **Cell transfection**

388 siRNA were transfected using INTERFERin (Polyplus Transfection) according to the
389 manufacturer's protocol. Briefly, 3x10⁵ cells per ml were seeded in 6-well plates and
390 transfected with 25 pmol/ml of control or ERRα siRNAs. Cells were harvested 48 or 72
391 hours after transfection. Control siRNAs were from Thermo Fisher Scientific (medium
392 GC Stealth RNA interference negative control duplexes). siRNAs were from Eurogentec:
393 ERR#1(GGCAGAAACCUAUCUCAGGUU), ERR#2(GAAUGCACUGGUGUCACAUCUGCUG),

394 MAP4K4#A (GUAGCACACUCCAGAAACA), MAP4K4#B (GCGAAGGAGAGAACAAGAA).

395 Cells were harvested 48 or 72 hours after transfection.

396

397 **Biochemical reagents**

398 Y27632 dihydrochloride monohydrate (Sigma-Aldrich, Y0503) was used at 2.5; 5 or 10

399 μM ; Pyr1 (Lim K inhibitor) (a gift from Laurence Lafanechère, Institute for Advanced

400 Biosciences, Grenoble, France) was used at 1; 5 or 10 μM ; Blebbistatin (Sigma-Aldrich,

401 B0560) was used at 5 μM ; PF-06260933 dihydrochloride (Sigma-Aldrich, PZ0272) was

402 used at 0.25 or 0.5 μM ; and GNE495 (Clinisciences, HY-100343) was used at 1 μM . Cells

403 were pre-treated (Western blot, xCELLigence) for 1h30 at 37°C before cell lysis or cell

404 adhesion assay, or incubated (micropatterns) with these inhibitors for 4 h at 37°C

405 before fixation.

406

407 Additional M&M can be found in Supplemental File.

408

409 **References**

- 410 1. Gardel ML, Schneider IC, Aratyn-Schaus Y, Waterman CM. Mechanical Integration of Actin
411 and Adhesion Dynamics in Cell Migration. *Annu Rev Cell Dev Biol.* 2010;26:315-33.
- 412 2. Bravo-Cordero JJ, Hodgson L, Condeelis J. Directed cell invasion and migration during
413 metastasis. *Curr Opin Cell Biol.* 2012;24(2):277-83.
- 414 3. Ridley AJ. Cell Migration: Integrating Signals from Front to Back. *Science.*
415 2003;302(5651):1704-9.
- 416 4. Blanchoin L, Boujemaa-Paterski R, Sykes C, Plastino J. Actin dynamics, architecture, and
417 mechanics in cell motility. *Physiol Rev.* 2014;94(1):235-63.
- 418 5. De Pascalis C, Etienne-Manneville S. Single and collective cell migration: the mechanics of
419 adhesions. *Mol Biol Cell.* 2017;28(14):1833-46.
- 420 6. Ridley AJ. Rho GTPase signalling in cell migration. *Curr Opin Cell Biol.* 2015;36:103-12.
- 421 7. Lawson CD, Ridley AJ. Rho GTPase signaling complexes in cell migration and invasion. *J Cell*
422 *Biol.* 05 2018;217(2):447-57.
- 423 8. Guan X, Guan X, Dong C, Jiao Z. Rho GTPases and related signaling complexes in cell
424 migration and invasion. *Exp Cell Res.* 2020;111824.
- 425 9. Machacek M, Hodgson L, Welch C, Elliott H, Pertz O, Nalbant P, et al. Coordination of Rho
426 GTPase activities during cell protrusion. *Nature.* 2009;461(7260):99-103.
- 427 10. Martin K, Reimann A, Fritz RD, Ryu H, Jeon NL, Pertz O. Spatio-temporal co-ordination of
428 RhoA, Rac1 and Cdc42 activation during prototypical edge protrusion and retraction dynamics. *Sci*
429 *Rep.* 2016;6(1):1-14.
- 430 11. Seetharaman S, Etienne-Manneville S. Microtubules at focal adhesions – a double-edged
431 sword. *J Cell Sci.* 2019;132(19).
- 432 12. Spiering D, Hodgson L. Dynamics of the Rho-family small GTPases in actin regulation and
433 motility. *Cell Adhes Migr.* 2011;5(2):170-80.
- 434 13. Mizuno K. Signaling mechanisms and functional roles of cofilin phosphorylation and

435 dephosphorylation. *Cell Signal*. 2013;25(2):457-69.

436 14. Kanellos G, Frame MC. Cellular functions of the ADF/cofilin family at a glance. *J Cell Sci*.
437 2016;129(17):3211-8.

438 15. Gao X, Gao C, Liu G, Hu J. MAP4K4: an emerging therapeutic target in cancer. *Cell Biosci*.
439 2016;6.

440 16. Tripolitsioti D, Grotzer MA, Baumgartner M. The Ser/Thr Kinase MAP4K4 Controls Pro-
441 Metastatic Cell Functions. *J Carcinog Mutagen*. 2017;08(01).

442 17. Stehbens S, Wittmann T. Targeting and transport: how microtubules control focal adhesion
443 dynamics. *J Cell Biol*. 2012;198(4):481-9.

444 18. Yue J, Xie M, Gou X, Lee P, Schneider MD, Wu X. Microtubules regulate focal adhesion
445 dynamics through MAP4K4. *Dev Cell*. 2014;31(5):572-85.

446 19. Vitorino P, Yeung S, Crow A, Bakke J, Smyczek T, West K, et al. MAP4K4 regulates integrin-
447 FERM binding to control endothelial cell motility. *Nature*. 2015;519(7544):425-30.

448 20. Tripolitsioti D, Kumar KS, Neve A, Migliavacca J, Capdeville C, Rushing EJ, et al. MAP4K4
449 controlled integrin β 1 activation and c-Met endocytosis are associated with invasive behavior of
450 medulloblastoma cells. *Oncotarget*. 2018;9(33):23220-36.

451 21. Dwyer MA, Joseph JD, Wade HE, Eaton ML, Kunder RS, Kazmin D, et al. WNT11 expression is
452 induced by estrogen-related receptor alpha and beta-catenin and acts in an autocrine manner to
453 increase cancer cell migration. *Cancer Res*. 2010;70(22):9298-308.

454 22. Sailland J, Tribollet V, Forcet C, Billon C, Barenton B, Carnesecchi J, et al. Estrogen-related
455 receptor α decreases RHOA stability to induce orientated cell migration. *Proc Natl Acad Sci U S A*.
456 2014;111(42):15108-13.

457 23. Tam IS, Giguère V. There and back again: The journey of the estrogen-related receptors in
458 the cancer realm. *J Steroid Biochem Mol Biol*. 2016;157:13-9.

459 24. Horard B, Vanacker J-M. Estrogen receptor-related receptors: orphan receptors desperately
460 seeking a ligand. *J Mol Endocrinol*. 2003;31(3):349-57.

- 461 25. Ranhotra HS. The estrogen-related receptors in metabolism and cancer: newer insights. J
462 Recept Signal Transduct. 2018;38(2):95-100.
- 463 26. Ranhotra HS. Estrogen-related receptor alpha and cancer: axis of evil. J Recept Signal
464 Transduct. 2015;35(6):505-8.
- 465 27. Chang C, Kazmin D, Jasper JS, Kunder R, Zuercher WJ, McDonnell DP. The metabolic regulator
466 ERR α , a downstream target of HER2/IGF-1, as a therapeutic target in breast cancer. Cancer Cell.
467 2011;20(4):500-10.
- 468 28. Bianco S, Sailland J, Vanacker J-M. ERRs and cancers: Effects on metabolism and on
469 proliferation and migration capacities. J Steroid Biochem Mol Biol. 2012;130(3):180-5.
- 470 29. Ao A, Wang H, Kamarajugadda S, Lu J. Involvement of estrogen-related receptors in
471 transcriptional response to hypoxia and growth of solid tumors. Proc Natl Acad Sci U S A.
472 2008;105(22):7821-6.
- 473 30. Zou C, Yu S, Xu Z, Wu D, Ng C-F, Yao X, et al. ERR α augments HIF-1 signalling by directly
474 interacting with HIF-1 α in normoxic and hypoxic prostate cancer cells. J Pathol. 2014;233(1):61-73.
- 475 31. Stein RA, Gaillard S, McDonnell DP. Estrogen-related receptor alpha induces the expression
476 of vascular endothelial growth factor in breast cancer cells. J Steroid Biochem Mol Biol.
477 2009;114(1-2):106-12.
- 478 32. Zhang K, Lu J, Mori T, Smith-Powell L, Synold TW, Chen S, et al. Baicalin increases VEGF
479 expression and angiogenesis by activating the ERR α /PGC-1 α pathway. Cardiovasc Res.
480 2011;89(2):426-35.
- 481 33. Tennessen JM, Baker KD, Lam G, Evans J, Thummel CS. The Drosophila estrogen-related
482 receptor directs a metabolic switch that supports developmental growth. Cell Metab.
483 2011;13(2):139-48.
- 484 34. Cai Q, Lin T, Kamarajugadda S, Lu J. Regulation of glycolysis and the Warburg effect by
485 estrogen-related receptors. Oncogene. 2013;32(16):2079-86.
- 486 35. Carnesecchi J, Forcet C, Zhang L, Tribollet V, Barenton B, Boudra R, et al. ERR α induces H3K9

487 demethylation by LSD1 to promote cell invasion. *Proc Natl Acad Sci U S A*. 2017;114(15):3909-14.

488 36. Zhang L, Carnesecchi J, Cerutti C, Tribollet V, Périan S, Forcet C, et al. LSD1-ERR α complex
489 requires NRF1 to positively regulate transcription and cell invasion. *Sci Rep*. 2018;8(1):10041.

490 37. Vicente-Manzanares M, Choi CK, Horwitz AR. Integrins in cell migration – the actin
491 connection. *J Cell Sci*. 2009;122(2):199-206.

492 38. Juanes MA, Bouguenina H, Eskin JA, Jaiswal R, Badache A, Goode BL. Adenomatous polyposis
493 coli nucleates actin assembly to drive cell migration and microtubule-induced focal adhesion
494 turnover. *J Cell Biol*. 2017;216(9):2859-75.

495 39. Romero S, Le Clainche C, Gautreau AM. Actin polymerization downstream of integrins:
496 signaling pathways and mechanotransduction. *Biochem J*. 2020;477(1):1-21.

497 40. Agaësse G, Barbolat-Boutrand L, Sulpice E, Bhajun R, Kharbili ME I, Berthier-Vergnes O, et al.
498 A large-scale RNAi screen identifies LCMR1 as a critical regulator of Tspan8-mediated melanoma
499 invasion. *Oncogene*. 2017;36(4):446-57.

500 41. Deblois G, Smith HW, Tam IS, Gravel S-P, Caron M, Savage P, et al. ERR α mediates metabolic
501 adaptations driving lapatinib resistance in breast cancer. *Nat Commun*. 2016;7: 12156.

502 42. Vitorino P, Yeung S, Crow A, Bakke J, Smyczek T, West K, et al. MAP4K4 regulates integrin-
503 FERM binding to control endothelial cell motility. *Nature*. 2015;519(7544):425-30.

504 43. Baumgartner M, Sillman AL, Blackwood EM, Srivastava J, Madson N, Schilling JW, et al. The
505 Nck-interacting kinase phosphorylates ERM proteins for formation of lamellipodium by growth
506 factors. *Proc Natl Acad Sci U S A*. 2006;103(36):13391-6.

507 44. Ammirati M, Bagley SW, Bhattacharya SK, Buckbinder L, Carlo AA, Conrad R, et al. Discovery
508 of an in Vivo Tool to Establish Proof-of-Concept for MAP4K4-Based Antidiabetic Treatment. *ACS Med*
509 *Chem Lett*. 2015;6(11):1128-33.

510 45. Ndubaku CO, Crawford TD, Chen H, Boggs JW, Drobnick J, Harris SF, et al. Structure-Based
511 Design of GNE-495, a Potent and Selective MAP4K4 Inhibitor with Efficacy in Retinal Angiogenesis.
512 *ACS Med Chem Lett*. 2015;6(8):913-8.

513 46. Bardet P-L, Horard B, Laudet V, Vanacker J-M. The ERR α orphan nuclear receptor controls
514 morphogenetic movements during zebrafish gastrulation. *Dev Biol.* 2005;281(1):102-11.

515 47. Amano M, Nakayama M, Kaibuchi K. Rho-Kinase/ROCK: A Key Regulator of the Cytoskeleton
516 and Cell Polarity. *Cytoskelet Hoboken Nj.* 2010;67(9):545-54.

517 48. Tripolitsioti D, Kumar KS, Neve A, Migliavacca J, Capdeville C, Rushing EJ, et al. MAP4K4
518 controlled integrin β 1 activation and c-Met endocytosis are associated with invasive behavior
519 of medulloblastoma cells. *Oncotarget.* 2018;9(33).

520 49. Klapholz B, Brown NH. Talin – the master of integrin adhesions. *J Cell Sci.*
521 2017;130(15):2435-46.

522 50. Sun Z, Costell M, Fässler R. Integrin activation by talin, kindlin and mechanical forces. *Nat Cell*
523 *Biol.* 2019;21(1):25-31.

524 51. Petrie RJ, Doyle AD, Yamada KM. Random versus directionally persistent cell migration.
525 2010;28.

526 52. Ma M, Baumgartner M. Intracellular *Theileria annulata* Promote Invasive Cell Motility
527 through Kinase Regulation of the Host Actin Cytoskeleton. *PLoS Pathog.* 2014;10(3).

528 53. LeClaire LL, Rana M, Baumgartner M, Barber DL. The Nck-interacting kinase NIK increases
529 Arp2/3 complex activity by phosphorylating the Arp2 subunit. *J Cell Biol.* 2015;208(2):161-70.

530 54. Santhana Kumar K, Tripolitsioti D, Ma M, Grählert J, Egli KB, Fiaschetti G, et al. The Ser/Thr
531 kinase MAP4K4 drives c-Met-induced motility and invasiveness in a cell-based model of SHH
532 medulloblastoma. *SpringerPlus.* 2015;4(1):19.

533

Figure 1

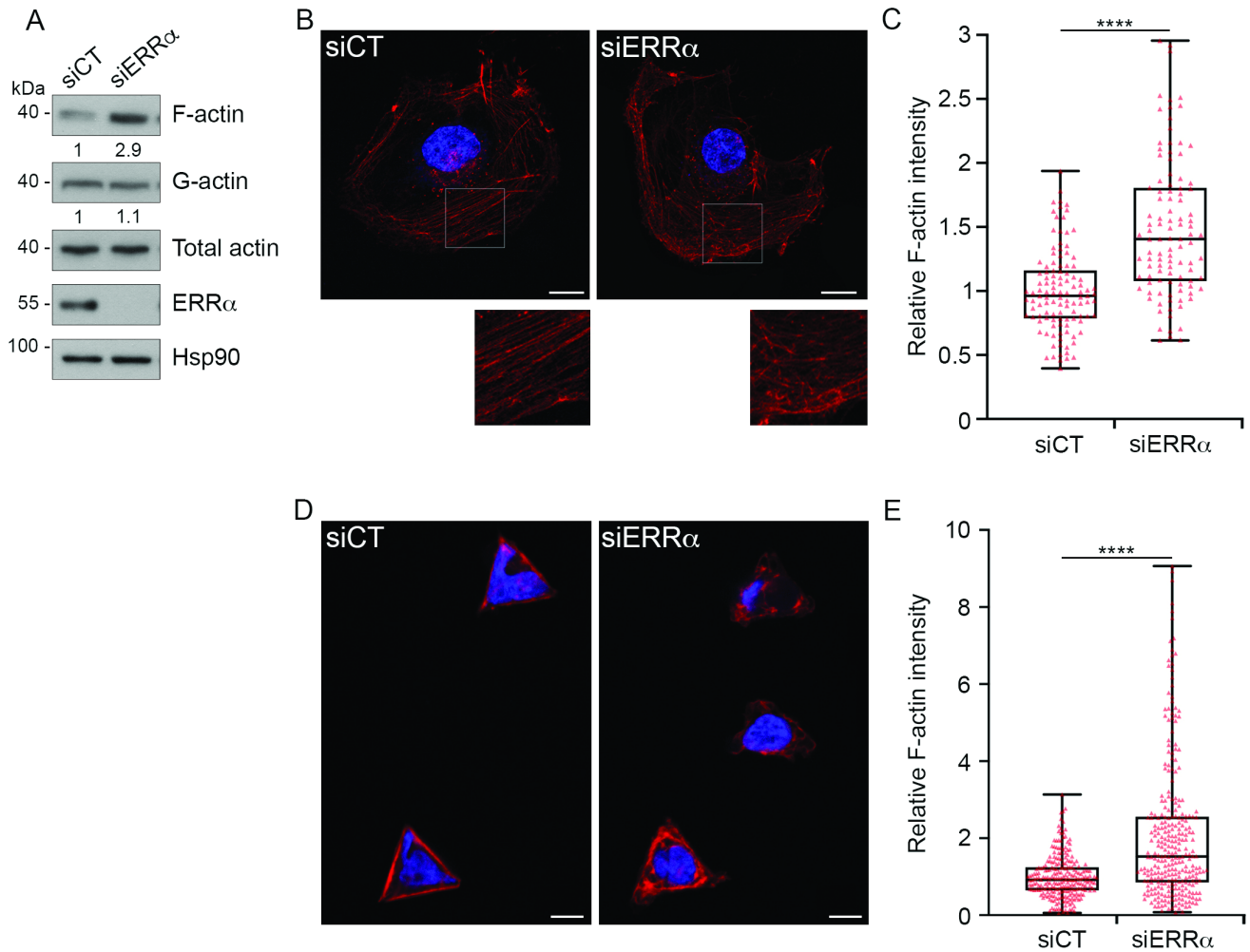


Figure 1: ERR α regulates actin polymerisation

(A) F-actin and G-actin from MDA-MB231 control and ERR α -depleted cells were segmented by ultra-speed centrifugation and analysed by western blot. Only one aliquot of each fraction was analysed by SDS-PAGE, which corresponded to 1% and 20% of the total volume of G-actin and F-actin fractions respectively. Quantifications of F-actin and G-actin are relative to total actin level and control conditions and representative of three independent experiments. (B) F-actin was stained using phalloïdin (red) in control and ERR α -depleted cells. Nuclei are shown in blue. The lower panels show a high magnification of the boxed regions in the image above. Scale bars: 20 μ m. (C) F-actin intensity was measured using ImageJ. (D) Triangle-shaped micropatterns were coated with 1,5 μ g/cm² of collagen I. Control or siERR α -transfected cells were then seeded onto micropatterns, F-actin was stained with SiR-actin (red) and nuclei were stained with Hoechst (blue). Scale bars: 10 μ m. (E) F-actin intensity was measured using ImageJ. Box-and-whisker plots are representative of 4 (C) or 9 (E) independent experiments. Mann-Whitney test, **** p <0.0001, $n \geq 25$ -30 cells per condition.

Figure 2

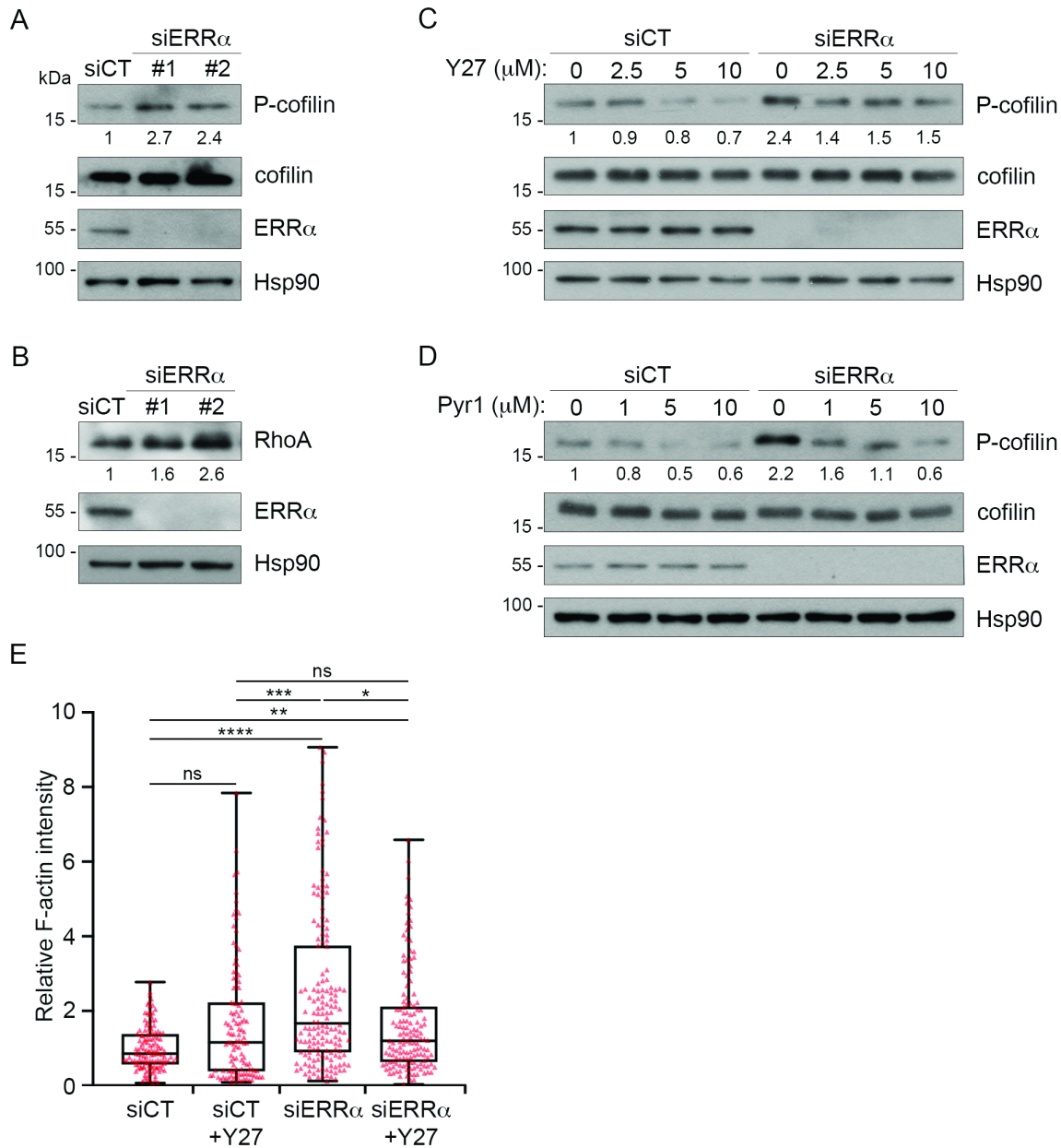


Figure 2: Modulation of the RhoA-ROCK-LIMK pathway rescues abnormal cofilin phosphorylation and F-actin accumulation due to ERR α depletion

(A) Expression of phosphorylated cofilin (P-cofilin), total cofilin, and (B) RhoA was analysed by western blot after MDA-MB231 cell transfection with control or ERR α siRNAs. (C) Control or ERR α -depleted cells were treated either with Y27632 or (D) Pyr1 as indicated, and subjected to western blot for analysis of P-cofilin and cofilin expression. (A, C, D) Quantifications indicate the ratio of P-cofilin/cofilin. (A, B, C, D) Hsp90 is used as a loading control and as the reference for quantification relative to control conditions. Quantifications are representative of three independent experiments. (E) Control or ERR α -depleted cells were seeded onto triangle-shaped micropatterns pre-coated with 1,5 μ g/cm² of collagen I and treated with 5 μ M Y27632. F-actin was stained with SiR-actin (red), and intensity was quantified using ImageJ. The box-and-whisker plot is representative of 5 independent experiments. Kruskal-wallis with Dunn's multiple comparisons test, ns (not significant) for $p > 0.05$, * $p < 0.05$ and **** $p < 0.0001$, $n \geq 25$ -30 cells per condition.

Figure 3

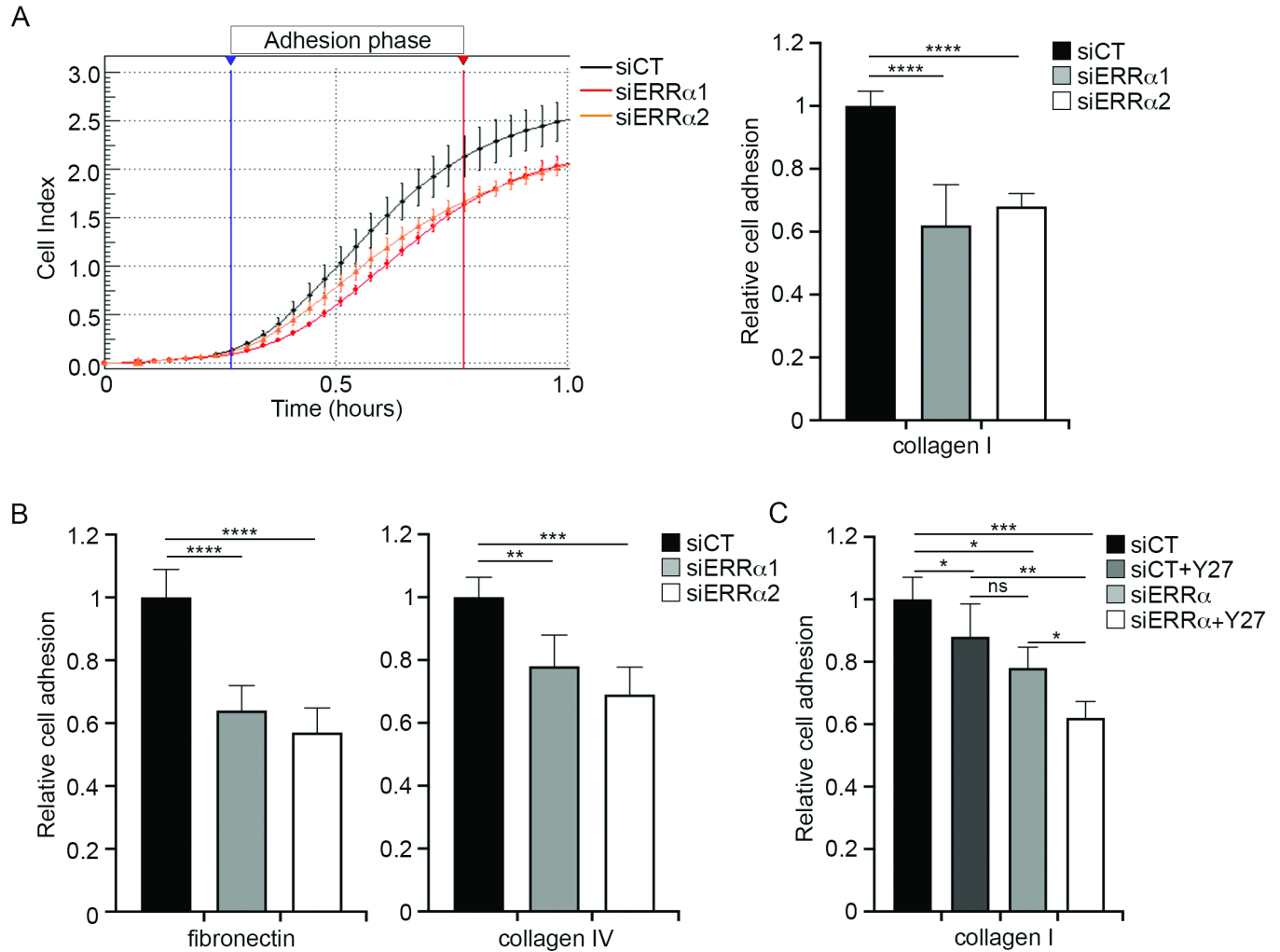


Figure 3: ERR α promotes cell adhesion, independently of its function in modulation of actin polymerisation. Cell–matrix adhesion was analysed after siRNA inhibition of ERR α expression using the xCELLigence system, which measure electrical impedance induced by cells across microelectrodes integrated on the bottom of 16-well culture plates (E-plate). The impedance signal is proportional to the intensity of the interactions exerted by the cells on the substrate. (A) E-plates were coated with 1.5 $\mu\text{g}/\text{cm}^2$ of collagen I. Control or ERR α -depleted cells were then seeded in E-plate for measurement of impedance, represented by the cell index (left panel) and the slope (right panel). Adhesion phase slopes, indicated as “Relative cell adhesion”, were calculated from the linear phase in a specific interval of time (blue and red arrowheads, left panel). (B) E-plates were coated with 1.5 $\mu\text{g}/\text{cm}^2$ of fibronectin or collagen IV. Control or ERR α -depleted cells were then seeded in E-plate for measurement of impedance. (C) Control or ERR α -depleted cells were treated with 5 μM Y27632 and seeded in E-plates pre-coated with 1.5 $\mu\text{g}/\text{cm}^2$ of collagen I for measurement of impedance. (A, B and C) Results are shown as mean \pm SEM of three or four independent experiments performed in quadruplicate. 2-way ANOVA with Dunnett's multiple comparisons, ns (not significant) for $p > 0.05$, * $p < 0.05$, ** $p < 0.01$, *** $p < 0.001$ and **** $p < 0.0001$.

Figure 4

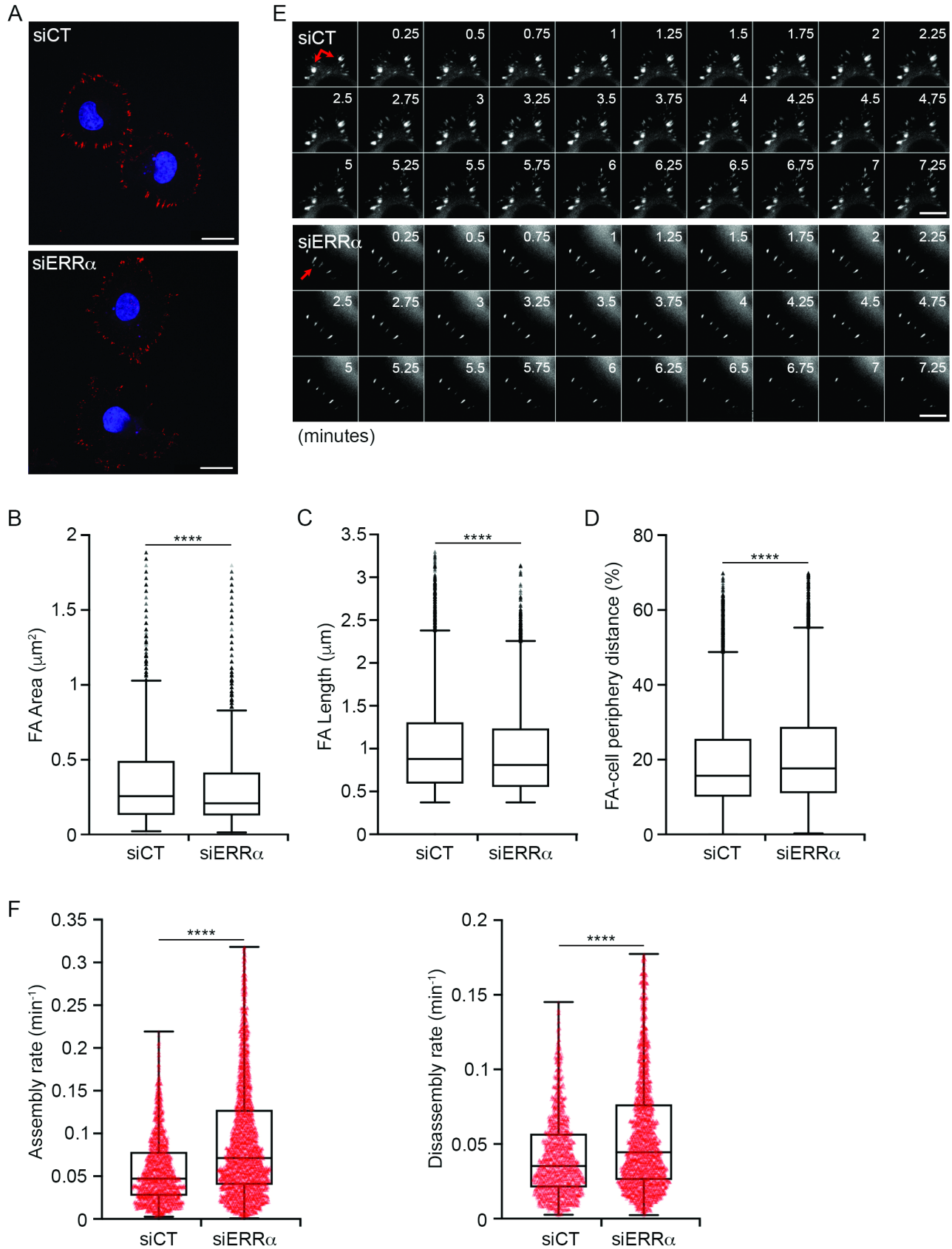


Figure 4: Loss of ERR α alters FA formation and dynamic

(A) MDA-MB231 control or ERR α -depleted cells were fixed and stained with vinculin for focal adhesions (red) and Hoechst for nuclei (blue). Scale bars: 20 μm . (B) Area, (C) length of FA and (D) relative distance to the cell periphery were visualized with vinculin staining, analysed using a Matlab code developed by R. Demets and M. Balland, and represented by box-and-whisker plots. Data correspond to four (D) or six (B, C) independent experiments. (E) Representative time-lapse images (montages) of FA dynamic in control or ERR α -depleted cells. Red arrows point to the FAs of interest. Scale bars: 10 μm . (F) Box-and-whisker plots show the assembly and disassembly rates of FA in ERR α -depleted cells relative to the control cells quantified with the Focal Adhesion Analysis (FAAS) method. Data are representative of three independent experiments. (B, C, D and F) Mann-Whitney test, **** $p < 0.0001$, $n \geq 25$ -30 cells and ≥ 470 FA per condition.

Figure 5

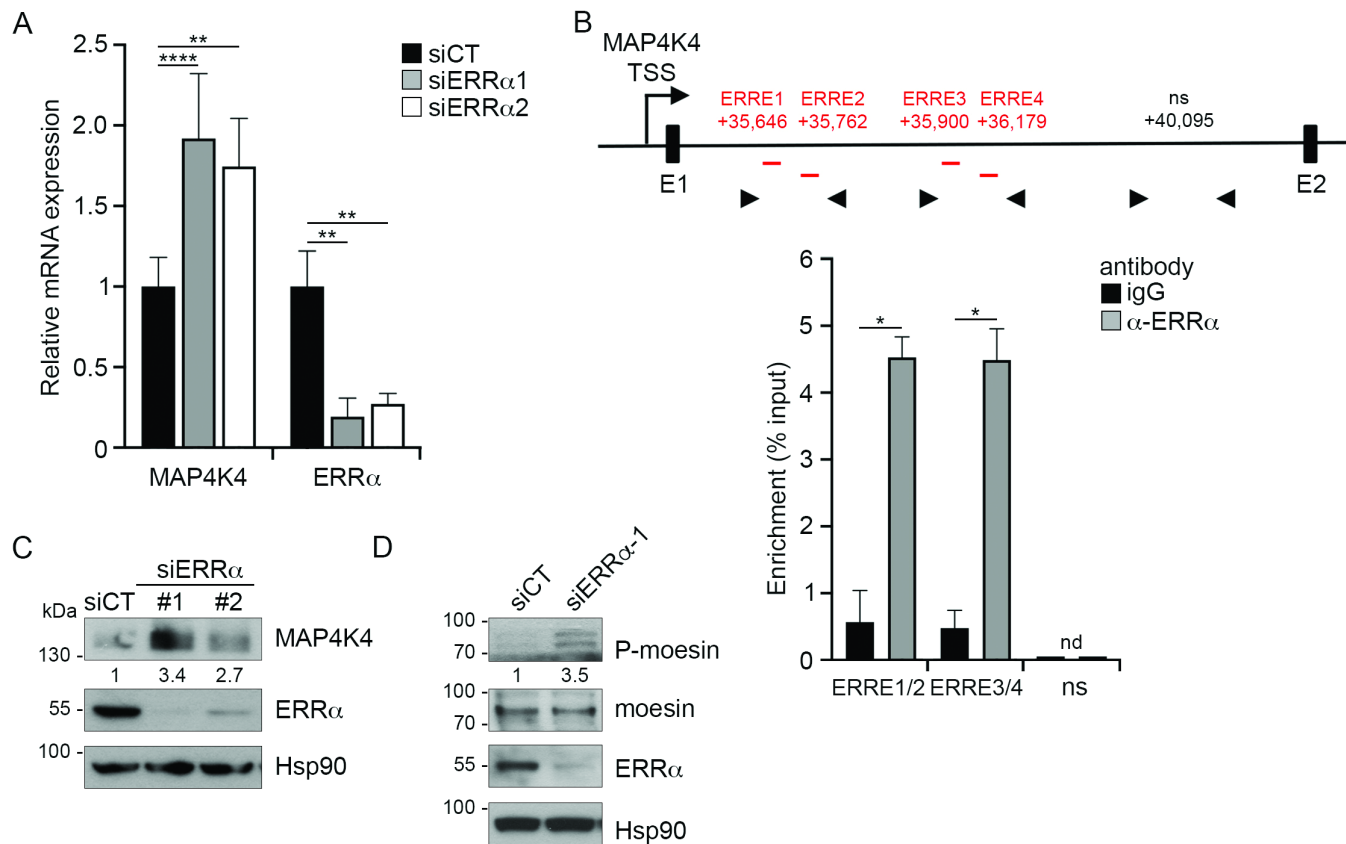


Figure 5: MAP4K4 is a novel target gene of ERRα

(A) The expression of MAP4K4 and ERRα genes was analysed by RT-qPCR after transfection with control or ERRα siRNA of MDA-MB231 cells. Data are mean ± SEM of three experiments performed in triplicate. 2-way ANOVA with Dunnett's multiple comparisons, **p<0.01 and ****p<0.0001. (B) The position of the putative ERRα binding regions (red letters) was indicated relative to the transcriptional start site (TSS) (upper panel). Arrowheads: oligonucleotide primers used in qPCR. Note that the scheme is not to scale. ChIP experiments were performed using anti-ERRα antibody or IgG (lower panel). Percent enrichments relative to input were measured by qPCR, amplifying a region encompassing the putative ERREs for ERRα. Data represent mean ± SEM of two experiments, each in duplicate. Mann-Whitney test, *p<0.05. nd, not detected. Non specific (ns) downstream region was used as a negative binding control. (C) Expression of MAP4K4 was analysed by western blot in control or ERRα-depleted cells. Quantifications are relative to Hsp90 levels and control conditions and representative of three independent experiments. (D) Expression of phosphorylated moesin (P-moesin) and total moesin was analysed by western blot. Quantifications indicate the ratio of P-moesin/moesin relative to control conditions and represent four independent experiments.

Figure 6

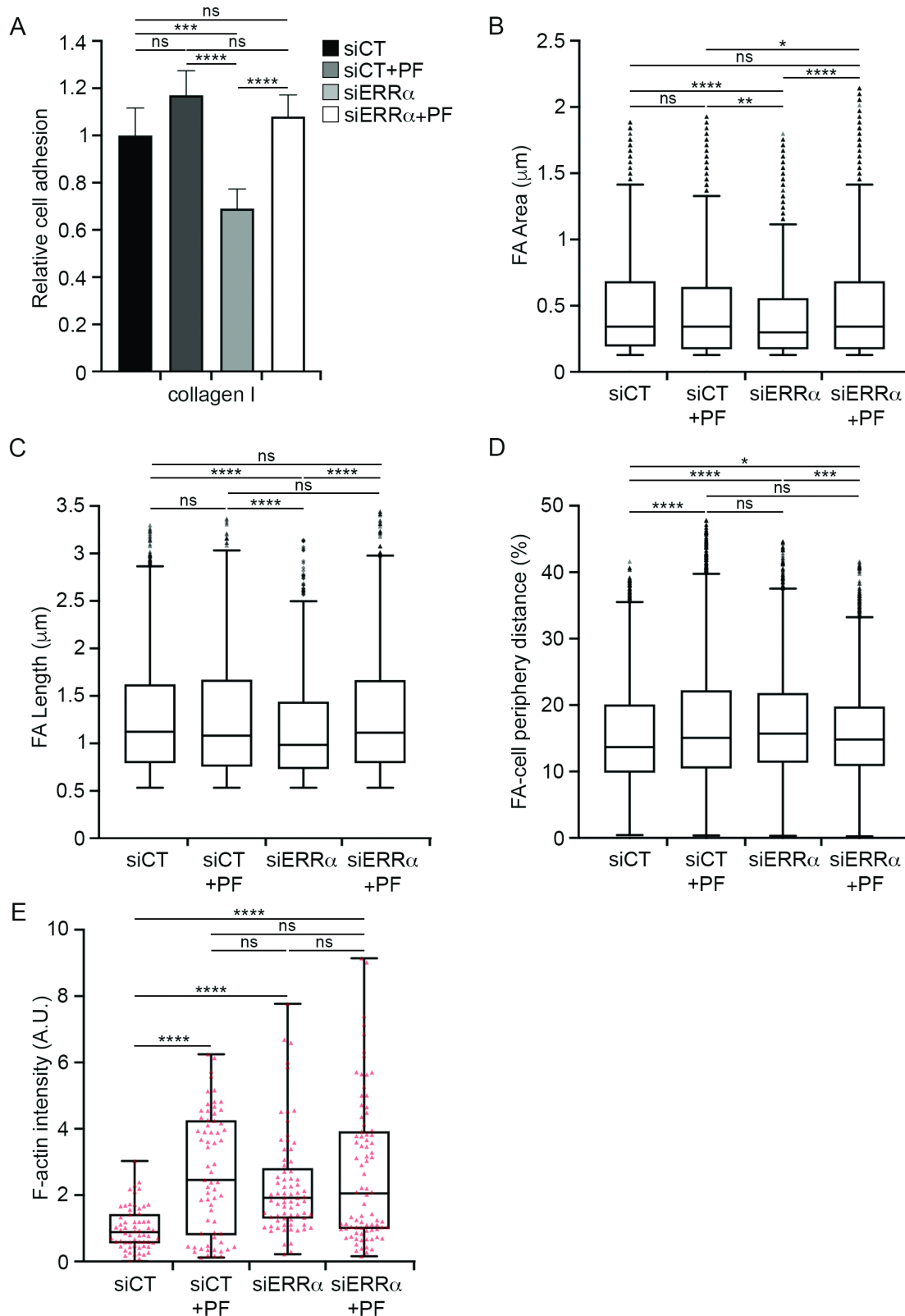


Figure 6: ERR α modulates cell adhesion and FA formation through MAP4K4

(A) Control or ERR α -depleted cells were treated with 0.5 μM PF-06260933 and seeded in E-plate pre-coated with 1.5 $\mu\text{g}/\text{cm}^2$ of collagen I. Then cell adhesion was measured using the xCELLigence system. Data are mean \pm SEM of four experiments performed in quadruplicate. 2-way ANOVA with Dunnett's multiple comparisons, ns (not significant) for $p > 0.05$, *** $p < 0.001$ and **** $p < 0.0001$. (B) Area (C) length of FA and (D) distance to the cell periphery were visualized with vinculin in control or ERR α -depleted cells treated with PF-06260933. FA analyses were performed using the Matlab algorithm developed by R. Demets and M. Balland. The box-and-whisker plots represent data of three independent experiments. (E) Control or ERR α -depleted cells were seeded onto triangle-shaped micropatterns pre-coated with 1,5 $\mu\text{g}/\text{cm}^2$ of collagen I and treated with 0.5 μM PF-06260933. F-actin was stained with SiR-actin (red), and intensity was quantified using ImageJ. Results are presented as a box-and-whisker plot and correspond to three independent experiments. Kruskal-wallis with Dunn's multiple comparisons test, ns (not significant) for $p > 0.05$, * $p < 0.05$, *** $p < 0.001$ and **** $p < 0.0001$, $n \geq 30$ cells and ≥ 670 FA per condition.

Figure S1

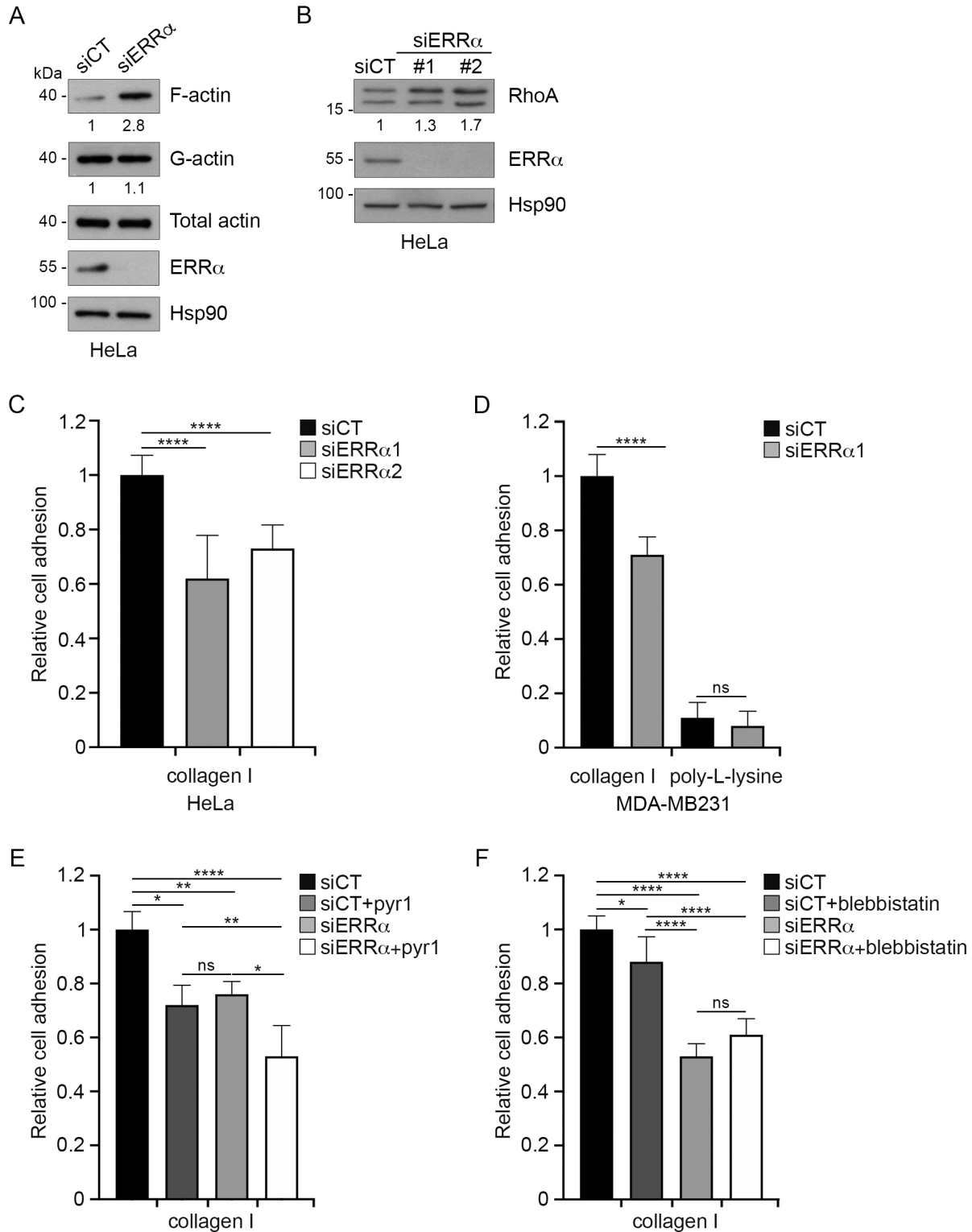


Figure S1: ERR α reduces actin polymerisation through the regulation of RhoA, and regulates cell adhesion independently of the RhoA pathway

(A) F-actin and G-actin from control and siERR α -transfected cells were segmented by ultra-speed centrifugation and analysed by western blot. Quantifications of F-actin and G-actin are relative to total actin level and control conditions and representative of three independent experiments. (B) Cells were transfected with control or siERR and subjected to western blot for analysis of RhoA expression. Quantifications are relative to Hsp90 levels and control conditions and representative of three independent experiments. (C) HeLa and (D) MDA-MB231 cells were transfected with control or siERR α and seeded in E-plate pre-coated with 1.5 $\mu\text{g}/\text{cm}^2$ of collagen I or 3 $\mu\text{g}/\text{cm}^2$ poly-L-lysine. Cell-adhesion was then analysed using the xCELLigence system. Data are mean \pm SEM of three independent experiments performed in quadruplicate. (E, F) Control or ERR α -depleted cells were treated with 5 μM Pyr1 (E) or 5 μM blebbistatin (F) and seeded in E-plates pre-coated with 1.5 $\mu\text{g}/\text{cm}^2$ of collagen I for measurement of impedance. Results are shown as mean \pm SEM of three or four independent experiments performed in quadruplicate. 2-way ANOVA with Dunnett's multiple comparisons, ns (not significant) for $p > 0.05$, * $p < 0.05$, ** $p < 0.01$ and **** $p < 0.0001$.

Figure S3

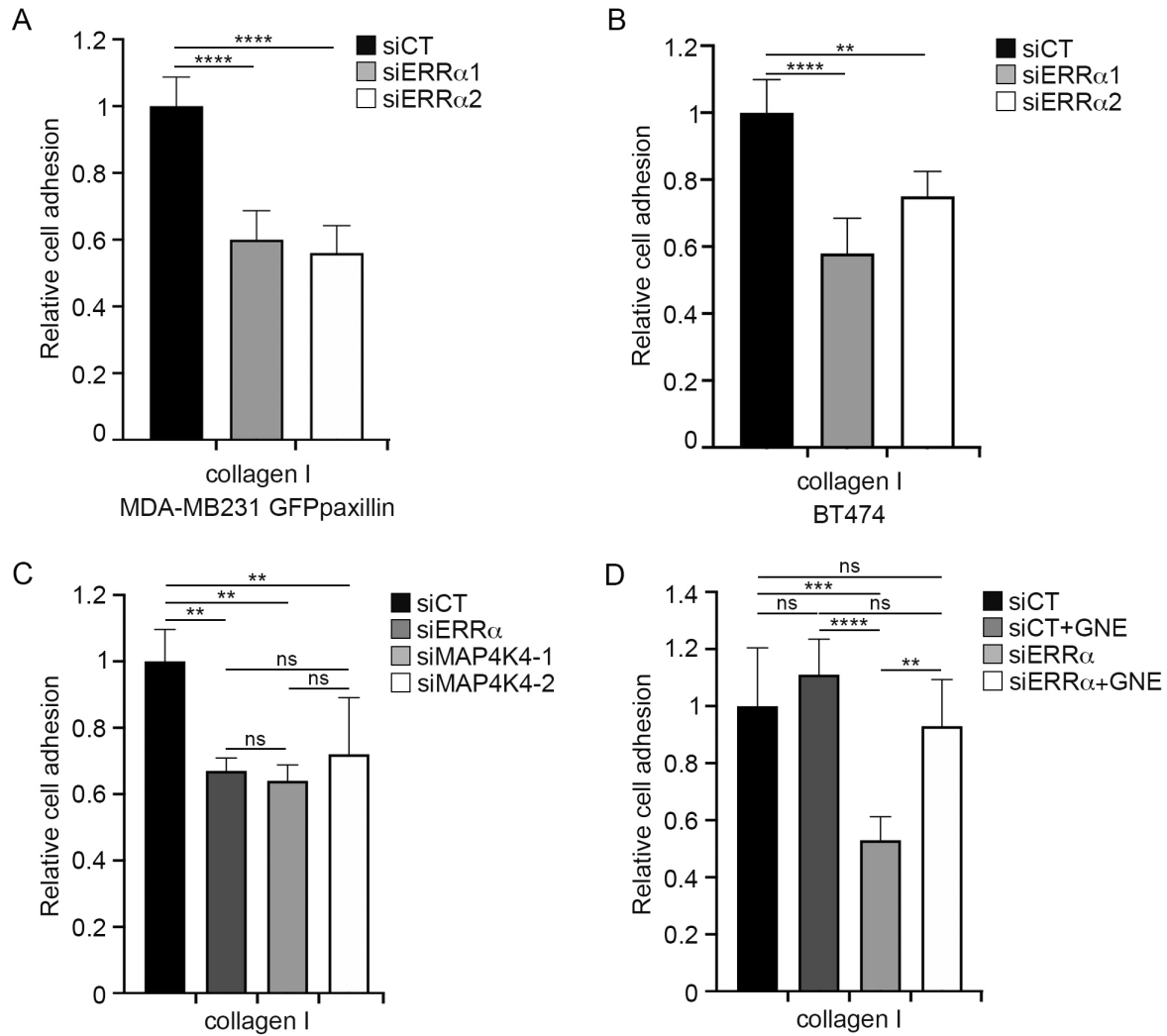
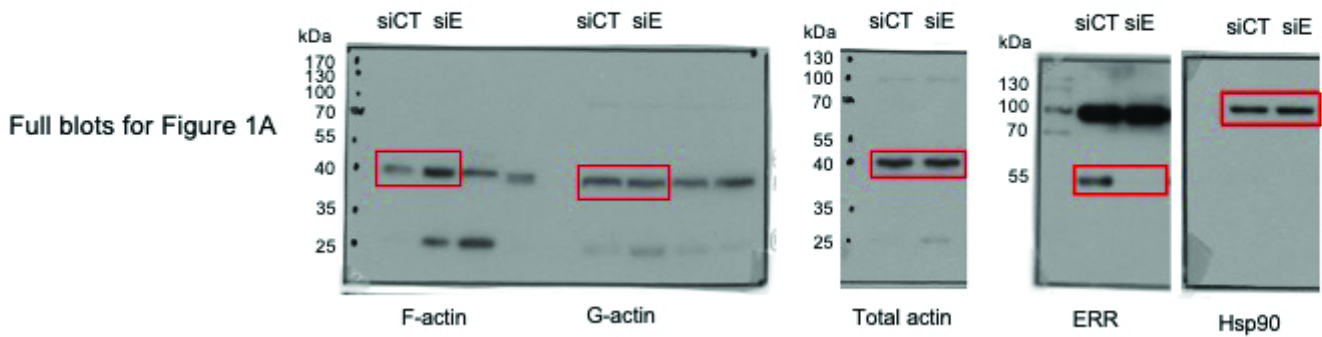


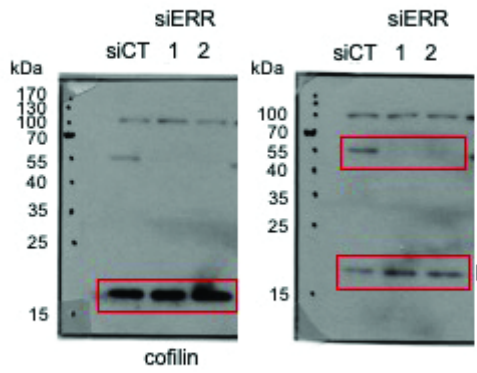
Figure S3: ERR α stimulates cell adhesion through the regulation of MAP4K4

(A) MDA-MB231 GFP-paxillin and (B) BT474 cells were transfected with control or siERR α and seeded in E-plate pre-coated with 1.5 $\mu\text{g}/\text{cm}^2$ of collagen I. Cell-adhesion was analysed using the xCELLigence system. Data are mean \pm SEM of three independent experiments performed in quadruplicate. (C, D) Control, ERR α - and MAP4K4-depleted cells (C) or control and ERR α -depleted cells treated with 1 μM GNE495 (D) were seeded in E-plates pre-coated with 1.5 $\mu\text{g}/\text{cm}^2$ of collagen I for measurement of impedance. Data are mean \pm SEM of three experiments performed in quadruplicate. 2-way ANOVA with Dunnett's multiple comparisons, ns (not significant) for $p > 0.05$, ** $p < 0.01$, *** $p < 0.001$ and **** $p < 0.0001$.

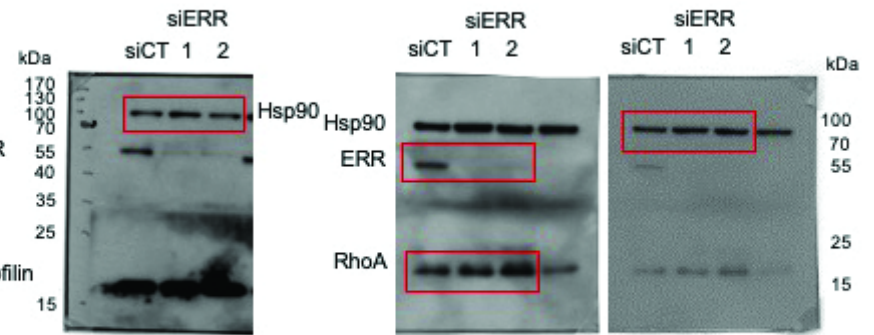
Figure S4



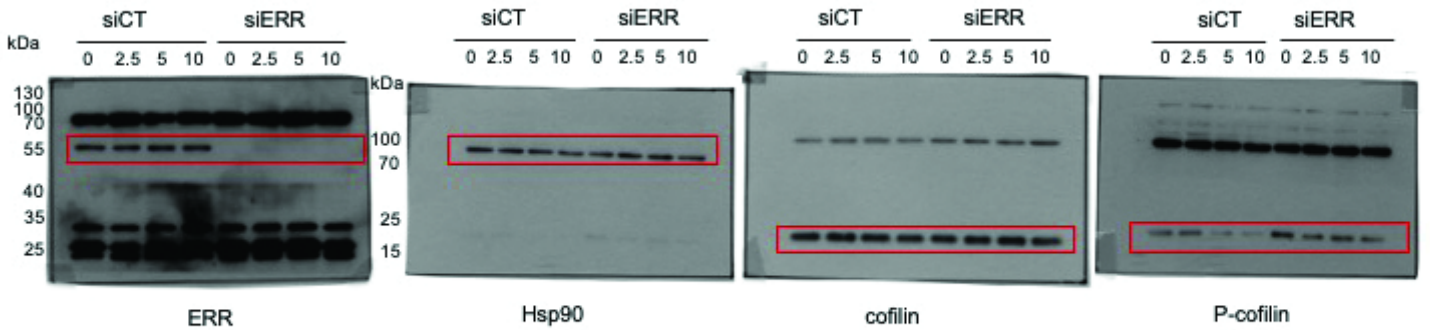
Full blots for Figure 2A



Full blots for Figure 2B



Full blots for Figure 2C



Full blots for Figure 2D

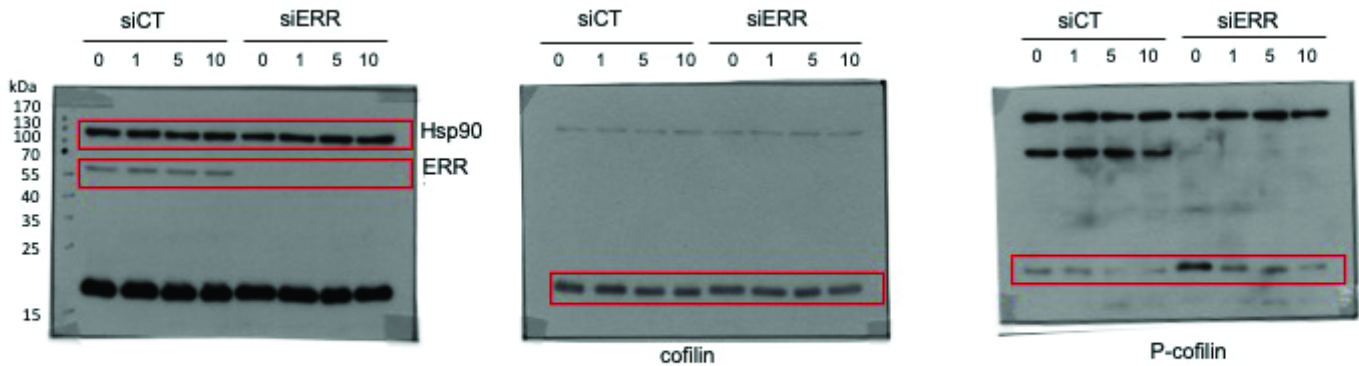
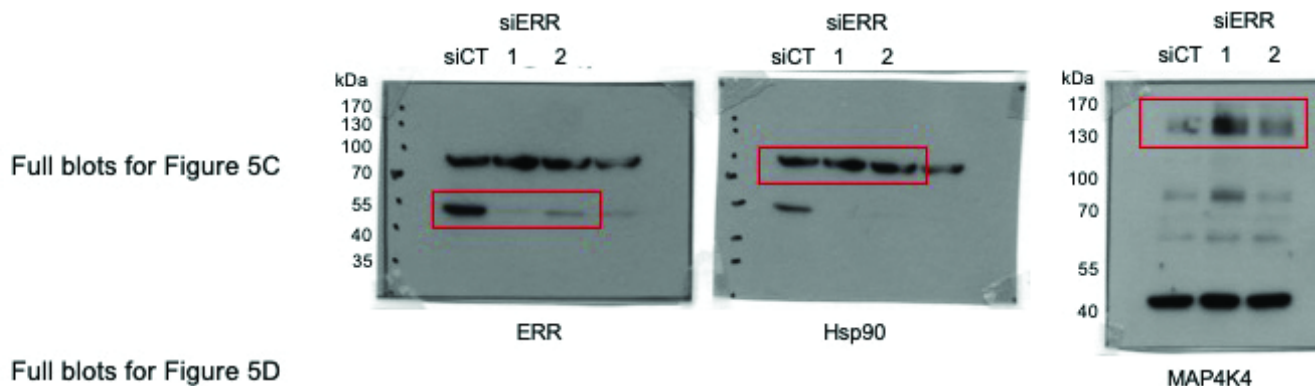


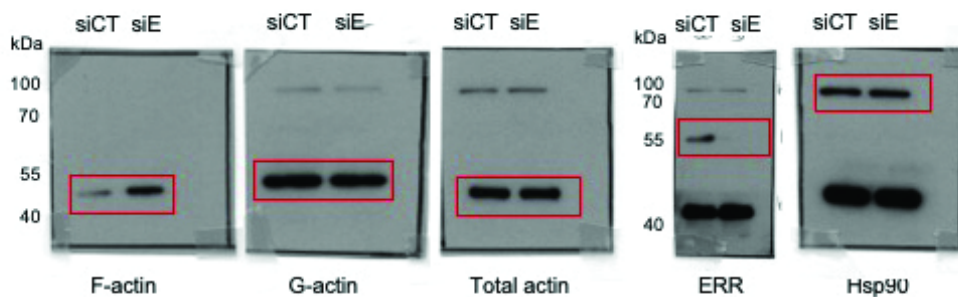
Figure S5



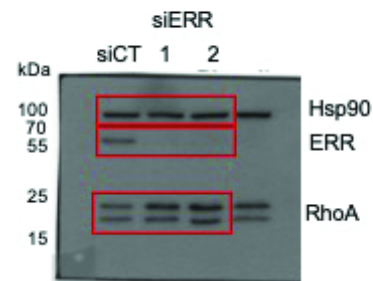
Full blots for Figure 5D



Full blots for Figure S1A



Full blots for Figure S1B



Full blots for Figure S2D

